Mechanism of Silicon-Nanowire-Diode Orientation in DC Electric Fields

Minh-Thang Hoang,[1] Nishant Deshmukh,[2] Amar T. Mohabir,[2] Leonard C. Feldman,[3] Michael A. Filler,[2] and Jerry W. Shan[1]

[1)] *Department of Mechanical & Aerospace Engineering, Rutgers University, Piscataway, NJ 08854, USA*

[2)] *School of Chemical & Biomolecular Engineering, Georgia Institute of Technology, Atlanta, GA 30332, USA*

[3)] *Department of Physics & Astronomy, Rutgers University, Piscataway, NJ 08854, USA*

(*Electronic mail: Authors to whom correspondence should be addressed: jshan@soe.rutgers.edu, michael.filler@chbe.gatech.edu)

(Dated: May 5, 2023)

Doped semiconductor nanowires are emerging as next-generation electronic colloidal materials, and the efficient manipulation of such nanostructures is crucial for technological applications. In fluid suspension, pn nanowires (pn NWs), unlike homogeneous nanowires, have a permanent dipole, and thus experience a torque under an external DC field that orients the nanowire with its n-type end in the direction of the field. Here, we quantitatively measure the permanent dipoles of various Si nanowire pn diodes and investigate their origin. By comparing the dipoles of pn NWs of different lengths and radii, we show that the permanent dipole originates from non-uniform surface-charge distributions, rather than the internal charges at the p-n junction as was previously proposed. This understanding of the mechanism for pn NWs orientation has relevance to the manipulation, assembly, characterization, and separation of nanowire electronics by electric fields.

Fabricating complete nanowire devices requires methods to precisely control and manipulate their building blocks, such as semiconducting nanowires. Several methods to achieve this have been described during the past decades, such as electrophoresis[1], dielectrophoresis[2,3], magnetophoresis[4], acoustophoresis[5], and optical tweezers[6]. Among these techniques, electric-field-mediated (EFM) particle assembly is a promising candidate for manipulating nanowire ensembles and creating ordered structures. EFM is flexible and scalable, requires relatively simple electrodes, and can be used for both charged and uncharged particles. Furthermore, it offers a plethora of ways of rotating and translating particles.

Previous EFM studies have dealt primarily with homogeneous particles, with manipulation based on well-established electrokinetic theories for colloids[7–16]. Nanodevices require electronically doped structures such as p-n, p-i-n, p-n-p or n-p-n doping. Their rotational and translational behaviors under E-field are thus more complicated than homogeneous particles[17,18]. There are relatively few reports of EFM studies of doped structures. One example is the work of Lee *et al.* using DC electric fields to align fluid-suspended pn NWs across an electrode pair[19]. Interestingly, all the NWs were oriented in the same direction, with their n-doped end pointed in the same direction as the DC field. These authors were able to build a half-wave rectifier and diode logic gates from a number of pn NWs.

The directed orientation observed by Lee *et al.* suggests that pn NWs have permanent dipoles that exist without the external electric field. However, the origin of the permanent dipole is unclear, and it is not known how it changes with parameters such as NW length, radius, depletion width, built-in voltage, etc. The focus of this work is to measure the permanent dipole of pn NWs in liquid suspension and to determine its origin. We have applied our technique to pn NWs of different lengths and radii. The measurements suggest that the permanent dipole is the result of a nonuniform surface-charge distribution, arising from the difference in the surface-charge density of the p and n sections.

Fig. 1a shows the schematic of our experiment. Two pairs of tantalum electrodes were used to form a square well on top of a glass slide. The wire electrodes generated spatially uniform electric fields across the solution, which contains pn NWs dispersed in low-conductivity solvents (mineral oil or n-methylpyrrolidone (NMP)). Such low-conductivity organic solvents mitigate the effect of electrolysis and induced-charge electrophoresis. We first applied 10 kHz AC voltage to one electrode pair to align the NWs with the $y-$direction. Then we applied a DC bias to the other electrode pair, subsequently orienting the NWs with the $x-$axis to observe the rotation and resulting orientation of pn NWs, as can be seen in Fig. 1c and 1d. The silicon pn NWs were grown using the vapor-liquid-solid (VLS) technique[20], and had lengths (L) ranging from 10 to 30 μm. The diameters (D) of the colloid catalysts were 50, 100 or 150 nm. As the nanowire average diameter differs by less than 13% from the catalyst diameter, we equate the diameters of the nanowires with parameter D. Each NW had an axially arranged boron- and phosphorous- doped section. The diodes showed clear rectification as expected for pn diodes (see supplemental figure Fig. S1c for the $I-V$ curve).

The electric-field-induced rotation of a suspended pn NW under a DC field can be described by the balance between the total electrostatic torque and the viscous resistance to rotation:

$$\begin{aligned}\gamma\dot{\theta} &= -(\tau_p + \tau_i) = (\boldsymbol{p}_{\text{perm}} \times \boldsymbol{E} + \boldsymbol{p}_{\text{induced}} \times \boldsymbol{E}) \\ &= -\left(p_{\text{perm}} E sin\theta + \alpha E^2 sin\theta cos\theta\right) \boldsymbol{e}_z \end{aligned} \quad (1)$$

where θ is the angle between the principal axis of the NW and the electric field, $\gamma = \frac{\pi\mu L^3}{3[log(L/D)-0.8]}$ is the rotational friction coefficient of the NW in a fluid of viscosity μ[21], p_{perm} is the permanent dipole, α is the parallel component of the particle polarizability and E is the electric field.

The left-hand side of Eqn. 1 is the viscous resistance to rotation. The first term to the right of the first equality, τ_p, is the torque by the electric field acting on the permanent dipole, and the second term, τ_i, is the electric torque due to the induced dipole. The rotation of the pn NW will be dictated by

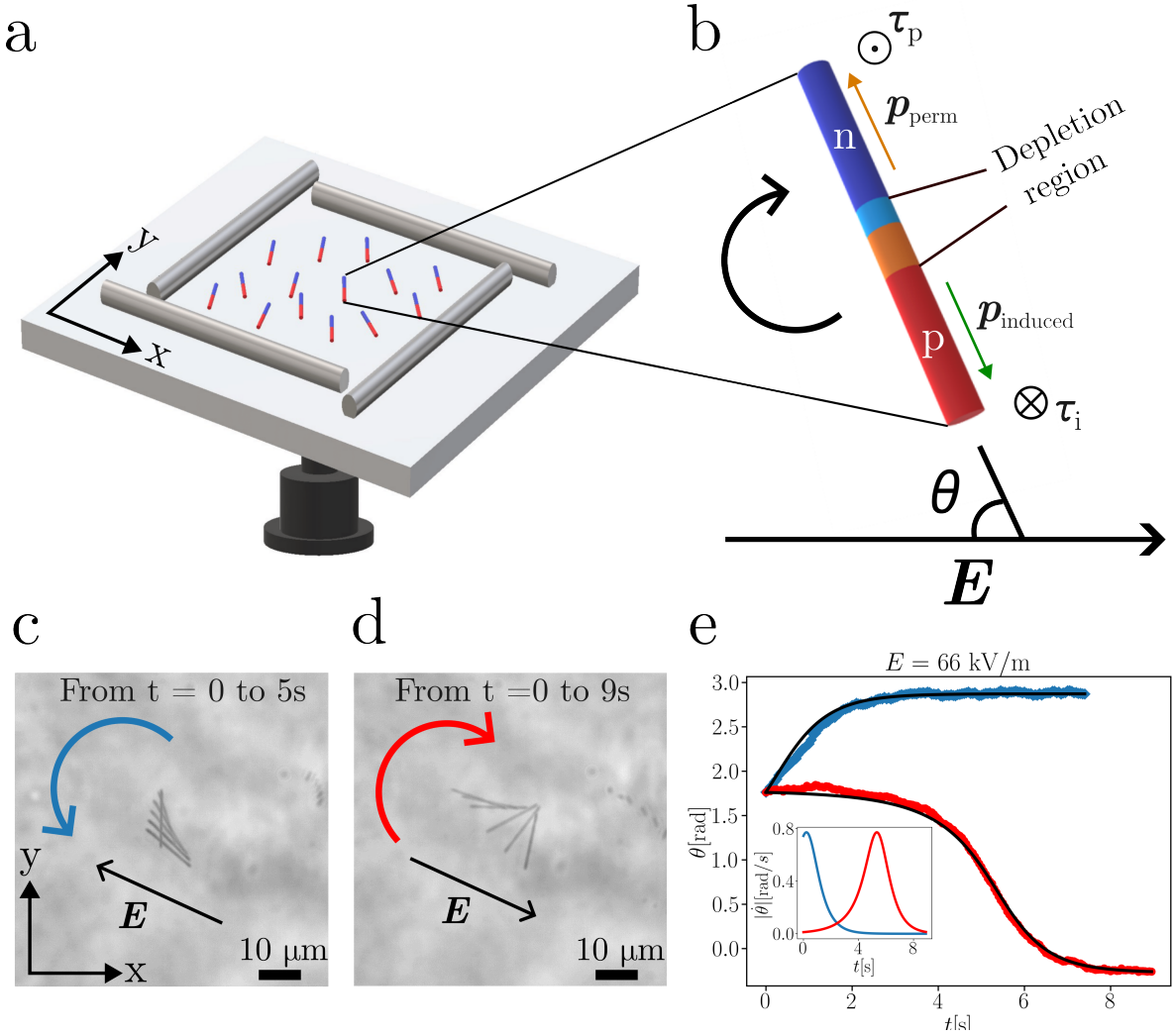

FIG. 1. (a) Schematic of experimental setup to study orientation of fluid-suspended pn NWs by DC electric fields. (b) Permanent and induced dipoles of a pn NW. If the two dipoles point in opposite directions, as depicted here, the relative strength of p_{perm} and $p_{induced}$ will dictate which direction the wire rotates. For fields below E_{crit}, p_{perm} will be the dominant torque, and the pn NW will orient with its p end in the field direction. (c) CCW rotation of pn nanowire when a DC field was applied across solution. (d) CW rotation when the polarity of E was reversed. (e) The time evolution of θ for a representative pn NW at E = 66 kV/m. Blue line and red line represent CCW and CW rotation, respectively. The data was fitted to Eqn. 1 to find p_{perm} and α. Inset is the corresponding rotation rate.

the relative strength of these two torques, which can point in the same or different directions (Fig. 1b). Because they scale as E and E^2, respectively, below a critical field strength, τ_p will dominate the rotation relative to τ_i. The NW should then rotate and orient its permanent dipole in the direction of E. If we change the polarity of the DC electric field, the particle will also change its direction of rotation because τ_p changes sign. This also means the pn NW can rotate an obtuse angle, *i.e.*, greater than 90°. This distinguishes a pn NW from homogeneous NWs, which can only rotate an acute angle under the induced dipole alone. At higher field strengths, τ_i dominates due to its quadratic dependence on E. The pn NW is then expected to lose its directed-rotation: it should simply align its principal axis with the field direction, rather than orienting with a particular end in the direction of the field.

In our experiments, the observed rotational behavior of the pn NWs closely followed the predictions of Eqn. 1, as illustrated in Fig. 1c-e. Fig 1c shows the counter-clockwise (CCW) rotation of the pn NW when a moderate E was applied across the solution. Upon changing the direction of E, the NW rotated clockwise (CW), and by more than 90 degrees, as can be seen in Fig. 1d. We also noted that in the beginning of the rotation, the rate was slower in the latter case, because induced and permanent dipoles pointed in opposite directions, as can be seen in Fig. 1e. As we gradually increased the field strength, the NW maintained this directed-rotation until E exceeded 100 kV/m. The induced torque then became dominant, as depicted in Fig. 2a, making the NW always rotate an acute angle and simply aligning (rather than orienting) with the external field.

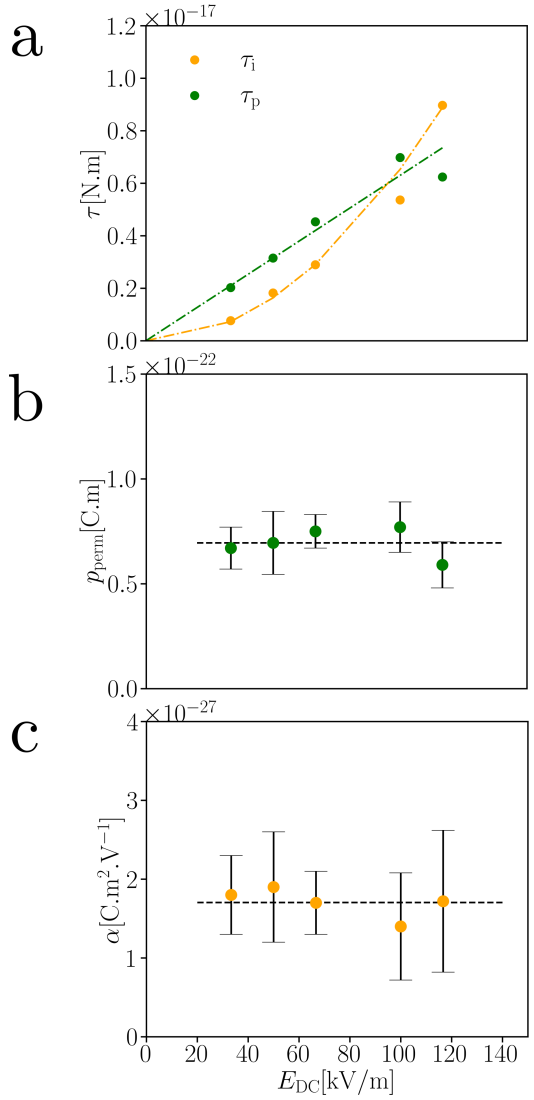

FIG. 2. The field dependence of EFM torques and dipoles of a representative pn NW. (a) Measured field dependence of τ_i (orange) and τ_p (green) (b) The extracted permanent dipole at different field strengths. (c) The extracted particle polarizability at different field strengths. 5 measurements were done at each field strength for b) and c).

To quantitatively find p_{perm}, we recorded the time evolution of the NW orientation angle, $\theta(t)$, at 5 different field strengths and fitted it to Eqn. 1. The fitting only involves two free parameters: permanent dipole moment p_{perm} and polarizability α. Fig. 1e shows the fitting for E=66 kV/m. At $t = 0$, the NW was kept perpendicular to the $x-$axis by an AC field. Then we turned this AC field off and applied a DC field to the other electrode pair. In one case, the NW rotated counter-clockwise (blue line), for τ_p and τ_i were in the same direction. We then flipped the DC field, such that the two torques had opposite directions and the NW rotated clockwise (red line). By fitting the rotation of the pn NW with the DC electric field in two different directions, we extract the permanent dipole, p_{perm}, of the NW, as well as the polarizatbility, α. Both p_{perm} and α are expected to be intrinsic properties of the pn NW, arising from their geometry, electronic properties, and surface properties, and thus should be independent of E. Fig. 2b-c clearly show that the extracted p_{perm} and α are independent of E over nearly an order of magnitude in field strength, as expected. This underscores the robustness of the measurement and fitting procedure.

A permanent dipole necessarily arises from separation of different charges. We now consider the origin of such charge differences.

At a semiconductor p-n junction, electrons in the n region diffuse to the p region to fill holes, leaving positive charges in the n section. Similarly, negative charges are formed in the p section due to diffusion of holes[22]. These opposite charges result in a dipole at the junction which points from p to n. The magnitude of this junction dipole scales with the cross sectional area and the built-in voltage, and is independent of the NW length. We can estimate this junction dipole using the depletion approximation[22] as

$$p_{\text{perm}}^{\text{junction}} = \pi R^2 \varepsilon_p \Psi_{bi} \tag{2}$$

where R is the particle radius, ε_p is the permittivity, and Ψ_{bi} is the built-in voltage of the pn NW. We have also conducted numerical simulation of the junction dipole using COMSOL Multiphysics and found excellent agreement with Eqn. 2, as detailed in the SI.

However, Eqn. 2 gives a permanent dipole that is 2 to 3 orders of magnitude lower than our measured dipole. We also measured dipoles of pn NWs having different lengths and radii to test Eqn. 2. Fig. 3a shows the variation of p_{perm} with length for 26 individual pn NWs. As seen in the figure, p_{perm} varied with L, which is not predicted by Eqn. 2. We also looked at NWs that were similar in length (from 14 - 17 μm), but had different diameters (colloid diameters of 50 nm vs. 150 nm). We found that p_{perm} scales with R instead of R^2 (Fig. 3b). This suggests that the measured p_{perm} does not originate from charges at the junction, as was previously proposed[19].

Instead, motivated by earlier work on heterogeneous colloids[23], we propose that the p_{perm} arises from a non-uniform surface-charge distribution on the NW. A pn NW dispersed in a liquid can develop surface-charge by absorbing ions from the liquid, or through dissociation of molecules. Even in low-conductivity fluids, charge can form at the particle surface, with charge densities[24,25] ranging from $10^9 - 10^{11}$ e.cm^{-2}. This process depends heavily on the surface chemistry of each part of the particle, and on the surface potential. Unfortunately, the surface potentials of p- and n-type Si NWs have not been measured in liquids like NMP and mineral oil, but measurements have been conducted in vacuum through Kelvin Probe Force Microscopy (KPFM)[26]. The KPFM measurements showed a higher surface potential on the n-type than on the p-type. This implies a higher surface-charge density on the n-type, and results in a surface p_{perm} pointing from p-type to n-type side, which agrees with both our observation in Fig. 4b and that of Lee *et al.*[19].

Assuming a uniform diameter for the n-type segment, and linear tapering of the p-type segment, the permanent dipole

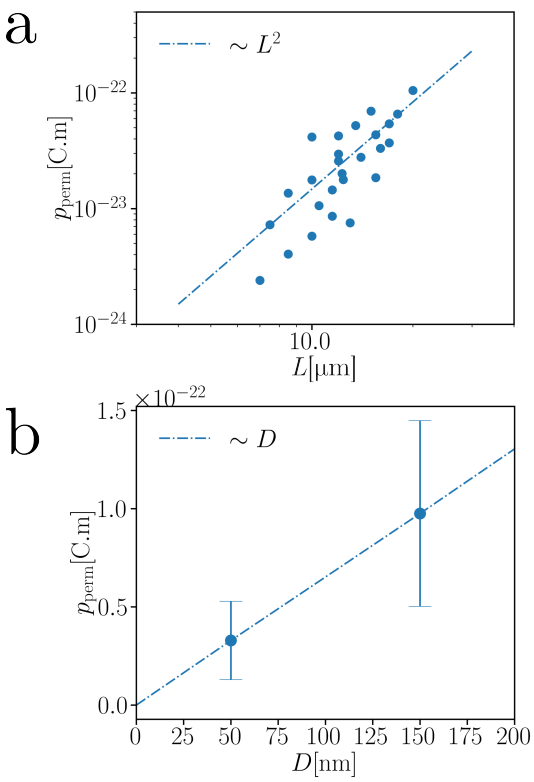

FIG. 3. Dependence of permanent dipoles on NW length and colloid diameter. (a) Measured permanent dipoles of nanowires that have same colloid diameter (100 nm) but different lengths. Dash line represents quadratic length dependence. (b) Measured permanent dipoles of 2 NW samples of different colloid diameters. All the pn NWs have lengths ranging from 14 - 17 μm.

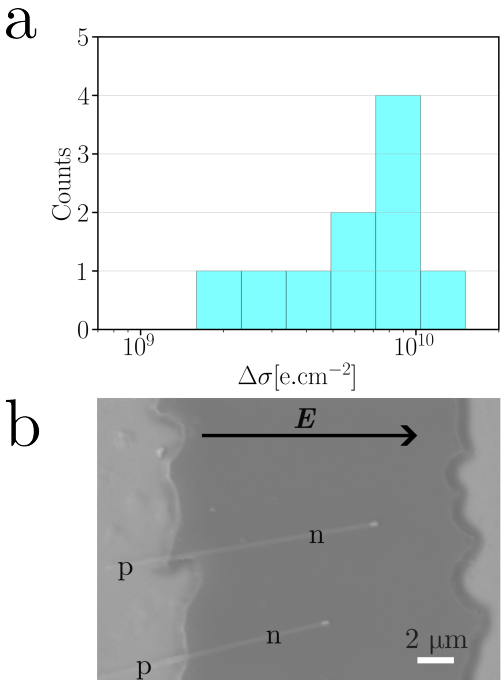

FIG. 4. Distribution of differences in charge across the pn NW, and demonstration of NW orientation by a DC field. (a) Distribution of measured $\Delta\sigma$ of pn NWs dispersed in NMP. The mean is $\langle\Delta\sigma\rangle = (7.04 \pm 3.53) \times 10^9$ e.cm^{-2}. (b) SEM image of pn NWs, oriented by a horizontal DC field generated by a pair of Pt electrodes. Since there is a higher surface-charge density on the n-type section of the NW, the permanent dipole points from p- to n type sections, and the NW orients with its n-type segment pointing in the direction of the DC E-field.

originating from this surface heterogeneity for a diode with equal-length p- and n- type segments would be:

$$p_{\text{perm}}^{\text{surface}} = \iint_S z\sigma dS = \frac{\pi\bar{R}L^2\Delta\sigma}{4} - \pi\Delta R L^2\Delta\sigma\frac{4\bar{R}+\Delta R}{24(4\bar{R}-\Delta R)}, \quad (3)$$

where σ is the surface-charge density, and $\Delta\sigma = \sigma_n - \sigma_p$ is the difference in surface-charge density between n- and p-type sections, $\bar{R}$ is the average radius, and ΔR is the change in radius within the p segment. The first term on the RHS is the dipole from the surface-charge heterogeneity for a cylindrical NW, and the second term is the geometrical correction due to tapering. As the correction is estimated to be about 25.86% of the first term for our nanowires, we can further simplify Eqn. 3 to $p_{\text{perm}}^{\text{surface}} \approx \frac{\pi\bar{R}L^2\Delta\sigma}{5.4}$. This surface permanent dipole, unlike the junction dipole, scales linearly with R and L^2. Thus, Eqn. 3 is in agreement with the experimental observations shown in Fig. 3.

Eqn. 3 also allows us to calculate $\Delta\sigma$ from the measured p_{perm}. The distribution of $\Delta\sigma$ for pn NWs in NMP is shown in Fig. 4a. To validate this result, we independently estimated the charge density of each section by doing ζ-potential measurements of two samples: homogeneous n-type and homogeneous p-type NWs with the same doping and growth conditions as the pn sample. The surface potential (Ψ) of each section can be approximated from the measured ζ: $\Psi_{\text{p}} \approx \zeta_{\text{p}} = 44.2 \pm 4.7$ mV and $\Psi_{\text{n}} \approx \zeta_{\text{n}} = 50.6 \pm 3.3$ mV. We then estimate the surface-charge density from the surface potential using Grahame equation[27].

$$\sigma = 2\varepsilon_s\kappa V_t sinh\left(\frac{\Psi}{2V_t}\right) \quad (4)$$

where $V_t = k_B T/e$ is the thermal voltage, ε_s and $1/\kappa$ are the permittivity and the Debye length of the fluid, respectively.

The estimated difference in surface-charge density, $\Delta\sigma$, from ζ-potential measurement is 7.7×10^9 e.cm^{-2}, which agrees well with that calculated from our experimental measurements of p_{perm} using Eqn. 3. Thus, the ζ-potential measurement supports the hypothesis that the p and n sections have different surface-charge densities, giving rise to the permanent dipole. Moreover, the higher ζ of the n-type NWs suggests that the permanent dipole should point from p side to n side, again in agreement with the direction of the dipole seen in Fig. 4b and also reported by Lee *et al.*[19]. Interestingly, this seems to hold for p- and n-doped Si dispersed in other liquids[28].

One can estimate the total surface-charge difference between n and p sections: $\Delta Q = \pi\Delta\sigma RL$. For 50-nm-radius

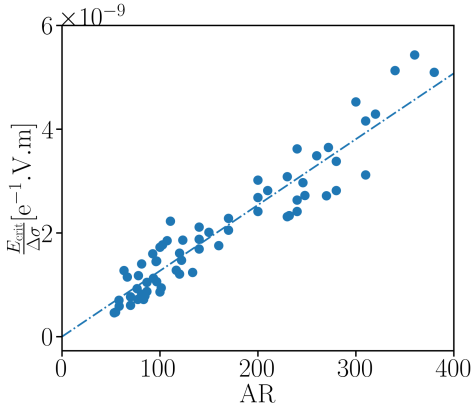

FIG. 5. Dependence of $E_{\text{crit}}/\Delta\sigma$ on aspect ratio. For each nanowire, its $\Delta\sigma$ and E_{crit} were measured by gradually increasing E and observe the rotation.

NWs, $\Delta Q \sim 80-200$ elementary charges. We note that when NWs are exposed to air or liquids, oxide layers are formed on its surfaces. The density of ionizable surface sites of SiO_2 is $\Gamma \approx 8$ nm^{-2}, *i.e.* there are about 10^6 ionizable sites on the surface of a 15 µm long wire[25]. Thus, only a very small difference (~ 0.015 %) in the ionizable sites is needed to generate the permanent dipoles that we observe. Furthermore, because there is only a small difference in the number of elementary surface-charges on the two halves of the pn NW, any randomness in the number and position of charged sites might lead to the variation of p_{perm} that we have observed in Fig. 4a between nominally identical diodes.

Due to the different scaling with E of the permanent and induced dipoles (Eqn. 1), there is a critical DC field strength for directed orientation of pn NWs. Below this E_{crit}, the nanowire will orient with a particular side pointing in the direction of the DC field, while above it, the pn NW will simply align with the field. By setting the LHS of Eqn. 1 to 0, we find that $E_{\text{crit}} \sim \Delta\sigma RL^2/R^2L = \Delta\sigma AR$, where AR is the aspect ratio of the NW. Thus, E_{crit} is expected to scale with the aspect ratio AR of the pn NW, *i.e.*, longer-aspect-ratio pn NWs can be more easily oriented with higher DC fields. We can test this experimentally for individual NWs by gradually decreasing E and observing their rotation to see when they stop orienting and begin simply aligning with the field. We have looked at 50-nm and 150-nm- diameter pn NWs, and found that, in general, E_{crit} increases with AR. As seen in Fig. 5, the measured ratios of $E_{\text{crit}}/\Delta\sigma$ collapse nicely in a straight line when plotted against NW aspect ratio, AR.

In summary, we have measured the permanent dipole of pn NWs with a contactless technique using DC electric fields to orient them in liquid suspension. By fitting the time evolution of θ to the torque-balance equation, we were able to quantify the permanent dipoles of pn NWs of different lengths and radii. More specifically, we have shown that this permanent dipole scales with R and L^2, and arises from a non-uniform surface-charge distribution. We want to highlight that our finding about the origin of p_{perm} is different than that previously proposed in the literature, *i.e.* that the dipole arises from the p-n junction[19]. Clearly, surface heterogeneity plays a crucial role in the orientation and assembly of pn NWs. The results also suggest that pn NWs can be made to rotate at different speeds in DC E-fields by applying different functionalizations to each section to change its surface chemistry and surface potential. This understanding of the mechanism for pn NW orientation may have relevance to pn-NW-based electric rotors, as well as enabling the efficient manipulation, assembly, characterization and separation of pn NWs by electric fields.

SUPPLEMENTARY MATERIAL

Refer to the supplementary material provided at {insert link} for comprehensive insights into experimental details, analytical procedures, and SEM images.

ACKNOWLEDGMENTS

This work was supported by the US National Science Foundation through grant CBET-2106579.

[1] D. Wu, J. Qin, and B. Lin, "Electrophoretic separations on microfluidic chips," J. Chromatogr. A **1184**, 542–559 (2008).
[2] T. Z. Jubery, S. K. Srivastava, and P. Dutta, "Dielectrophoretic separation of bioparticles in microdevices: A review," ELECTROPHORESIS **35**, 691–713 (2014).
[3] A. Castellanos, A. Ramos, A. González, N. G. Green, and H. Morgan, "Electrohydrodynamics and dielectrophoresis in microsystems: scaling laws," J. Phys. D: Appl. Phys. **36**, 2584–2597 (2003).
[4] M. Suwa and H. Watarai, "Magnetoanalysis of micro/nanoparticles: A review," Anal Chim Acta **690**, 137–147 (2011).
[5] S.-C. S. Lin, X. Mao, and T. J. Huang, "Surface acoustic wave (SAW) acoustophoresis: now and beyond," Lab Chip **12**, 2766 (2012).
[6] C. J. Bustamante, Y. R. Chemla, S. Liu, and M. D. Wang, "Optical tweezers in single-molecule biophysics," Nat Rev Methods Primers **1** (2021).
[7] L. Dong, J. Bush, V. Chirayos, R. Solanki, J. Jiao, Y. Ono, J. F. Conley, and B. D. Ulrich, "Dielectrophoretically Controlled Fabrication of Single-Crystal Nickel Silicide Nanowire Interconnects," Nano Lett. **5**, 2112–2115 (2005).
[8] M. Duchamp, K. Lee, B. Dwir, J. W. Seo, E. Kapon, L. Forró, and A. Magrez, "Controlled Positioning of Carbon Nanotubes by Dielectrophoresis: Insights into the Solvent and Substrate Role," ACS Nano **4**, 279–284 (2010).
[9] E. M. Freer, O. Grachev, X. Duan, S. Martin, and D. P. Stumbo, "High-yield self-limiting single-nanowire assembly with dielectrophoresis," Nature Nanotech **5**, 525–530 (2010).
[10] O. Englander, D. Christensen, J. Kim, L. Lin, and S. J. S. Morris, "Electric-Field Assisted Growth and Self-Assembly of Intrinsic Silicon Nanowires," Nano Lett. **5**, 705–708 (2005).
[11] D. Fan, Z. Yin, R. Cheong, F. Q. Zhu, R. C. Cammarata, C. L. Chien, and A. Levchenko, "Subcellular-resolution delivery of a cytokine through precisely manipulated nanowires," Nature Nanotech **5**, 545–551 (2010).
[12] C. S. Lao, J. Liu, P. Gao, L. Zhang, D. Davidovic, R. Tummala, and Z. L. Wang, "ZnO Nanobelt/Nanowire Schottky Diodes Formed by Dielectrophoresis Alignment across Au Electrodes," Nano Lett. **6**, 263–266 (2006).
[13] P. A. Smith, C. D. Nordquist, T. N. Jackson, T. S. Mayer, B. R. Martin, J. Mbindyo, and T. E. Mallouk, "Electric-field assisted assembly and alignment of metallic nanowires," Appl. Phys. Lett. **77**, 1399–1401 (2000).
[14] S. Raychaudhuri, S. A. Dayeh, D. Wang, and E. T. Yu, "Precise Semiconductor Nanowire Placement Through Dielectrophoresis," Nano Lett. **9**, 2260–2266 (2009).

[15]C. Akin, J. Yi, L. C. Feldman, C. Durand, S. M. Hus, A.-P. Li, M. A. Filler, and J. W. Shan, "Contactless Determination of Electrical Conductivity of One-Dimensional Nanomaterials by Solution-Based Electro-orientation Spectroscopy," ACS Nano **9**, 5405–5412 (2015).

[16]W. Yuan, G. Tutuncuoglu, A. Mohabir, L. Liu, L. C. Feldman, M. A. Filler, and J. W. Shan, "Contactless Electrical and Structural Characterization of Semiconductor Nanowires with Axially Modulated Doping Profiles," Small **15**, 1805140 (2019).

[17]E. T. Ritchie, D. J. Hill, T. M. Mastin, P. C. Deguzman, J. F. Cahoon, and J. M. Atkin, "Mapping Free-Carriers in Multijunction Silicon Nanowires Using Infrared Near-Field Optical Microscopy," Nano Lett. **17**, 6591–6597 (2017).

[18]B. Tian and C. M. Lieber, "Nanowired Bioelectric Interfaces," Chem. Rev. **119**, 9136–9152 (2019).

[19]C. H. Lee, D. R. Kim, and X. Zheng, "Orientation-Controlled Alignment of Axially Modulated pn Silicon Nanowires," Nano Lett. **10**, 5116–5122 (2010).

[20]Y. Wu, J. Xiang, C. Yang, W. Lu, and C. M. Lieber, "Single-crystal metallic nanowires and metal/semiconductor nanowire heterostructures," Nature **430**, 61–65 (2004).

[21]M. Doi and S. F. Edwards, *The Theory of Polymer Dynamics*, Vol. 73 (Oxford University Press, 1988).

[22]S. M. Sze and K. K. Ng, *Physics of Semiconductor Devices 3rd ed.* (Wiley-Interscience, 2006).

[23]J. L. Anderson, "Effect of nonuniform zeta potential on particle movement in electric fields," J. Colloid Interf. Sci. **105**, 45–54 (1985).

[24]F. Beunis, F. Strubbe, K. Neyts, and D. Petrov, "Beyond Millikan: The Dynamics of Charging Events on Individual Colloidal Particles," Phys. Rev. Lett. **108** (2012).

[25]G. Kokot, M. I. Bespalova, and M. Krishnan, "Measured electrical charge of SiO_2 in polar and nonpolar media," J. Chem. Phys. **145**, 194701 (2016).

[26]A. Doukkali, S. Ledain, C. Guasch, and J. Bonnet, "Surface potential mapping of biased pn junction with kelvin probe force microscopy: application to cross-section devices," Appl. Surf. Sci. **235**, 507–512 (2004).

[27]J. N. Israelachvili, *Intermolecular and Surface Forces* (Academic Press, 2011).

[28]L. Wang, Y. Gao, F. Dai, D. Kong, H. Wang, P. Sun, Z. Shi, X. Sheng, B. Xu, and L. Yin, "Geometrical and Chemical-Dependent Hydrolysis Mechanisms of Silicon Nanomembranes for Biodegradable Electronics," ACS Appl. Mater. Inter. **11**, 18013–18023 (2019).